Articles

Studies of Nucleoside Transporters Using Novel Autofluorescent Nucleoside Probes†

Jing Zhang,[§,||,¶] Xuejun Sun,[||,¶] Kyla M. Smith,[§,‡] Frank Visser,[§,||] Pat Carpenter,[§,||] Geraldine Barron,[||] Yunshan Peng,[#] Morris J. Robins,[#] Stephen A. Baldwin,[⊥] James D. Young,[§,‡] and Carol E. Cass*[,§,||]

Membrane Protein Research Group, Departments of Oncology and Physiology, University of Alberta, and Cross Cancer Institute, Edmonton, Alberta T6G 1Z2, Canada, Department of Chemistry and Biochemistry, Brigham Young University, Provo, Utah 84602-5700, and Astbury Centre for Structural Molecular Biology, Institute for Membrane and Systems Biology, University of Leeds, Leeds LS2 9JT, United Kingdom

Received October 9, 2005; Revised Manuscript Received November 28, 2005

ABSTRACT: To better understand nucleoside transport processes and intracellular fates of nucleosides, we have developed a pair of fluorescent nucleoside analogues, FuPmR and dFuPmR, that differ only in the sugar moiety (ribofuranosyl versus 2′-deoxy, respectively), for real-time analysis of nucleoside transport into living cells by confocal microscopy. The binding and transportability of the two compounds were assessed for five recombinant human nucleoside transporters (hENT1/2, hCNT1/2/3) produced in *Saccharomyces cerevisiae* and/or oocytes of *Xenopus laevis*. The ribosyl derivative (FuPmR) was used to demonstrate proof of principle in live cell imaging studies in 11 cultured human cancer cell lines with different hENT1 activities. The autofluorescence emitted from FuPmR enabled direct visualization of its movement from the extracellular medium into the intracellular compartment of live cells, and this process was blocked by inhibitors of hENT1 (nitrobenzylmercaptopurine ribonucleoside, dipyridamole, and dilazep). Quantitative analysis of fluorescence signals revealed two stages of FuPmR uptake: a fast first stage that represented the initial uptake rate (i.e., transport rate) followed by a slow long-lasting second stage. The accumulation of FuPmR and/or its metabolites in nuclei and mitochondria was also visualized by live cell imaging. Measurements of fluorescence intensity increases in nuclei and mitochondria revealed rate-limited processes of permeant translocation across intracellular membranes, demonstrating for the first time the intracellular distribution of nucleosides and/or nucleoside metabolites in living cells. The use of autofluorescent nucleosides in time-lapse confocal microscopy is a novel strategy to quantitatively study membrane transport of nucleosides and their metabolites that will provide new knowledge of nucleoside biology.

Integral membrane proteins mediate the passage of nucleosides, including anticancer and antiviral nucleoside analogues, across biological membranes (*1*, *2*). Two distinct nucleoside transporter families, the equilibrative nucleoside transporters (ENTs)[1] and the concentrative nucleoside transporters (CNTs), have been identified by molecular cloning and functional expression of cDNAs from a variety of sources, including mammals, protozon parasites, and bacteria. In human (h) cells and tissues, hENT1 and -2 mediate facilitated diffusion of nucleosides down their concentration gradients whereas hCNT1, -2 and -3 couple uphill transport of nucleosides to downhill transport of sodium ions and, in the case of hCNT3, also to downhill transport of protons.

† This research was funded by the National Cancer Institute of Canada (C.E.C., J.D.Y.), the Alberta Cancer Foundation (C.E.C., J.D.Y.), and pharmaceutical company gift funds (M.J.R.). C.E.C. is Canada Research Chair in Oncology, J.D.Y. is Heritage Scientist of the Alberta Heritage Foundation for Medical Research, and M.J.R. is J. Rex Goates Professor of Chemistry at Brigham Young University. Studentship support was from the Canadian Institutes of Health Research (J.Z.), the Alberta Heritage Foundation for Medical Research (J.Z., F.V.), the Department of Oncology Endowed Studentship (J.Z., F.V.), and the J. S. Bradshaw Graduate Research Fellowship at Brigham Young University (Y.P.).

* Address correspondence to Dr. Carol E. Cass, Department of Oncology, Cross Cancer Institute, 11540 University Ave., Edmonton, Alberta, Canada T6G 1Z2. Tel, 780-432-8320; fax, 780-432-8425; e-mail, carol.cass@cancerboard.ab.ca.

§ Membrane Protein Research Group.

|| Department of Oncology, University of Alberta, and the Cross Cancer Institute.

¶ These authors made equal contributions to the work presented here.

‡ Department of Physiology, University of Alberta.

Brigham Young University.

⊥ University of Leeds.

[1] Abbreviations: ENT, equilibrative nucleoside transporter; CNT, concentrative nucleoside transporter; h, human; NBMPR, nitrobenzylmercaptopurine ribonucleoside; IC_{50}, inhibitory concentration 50%; K_i, inhibitory constant; FRAP, fluorescence recovery after photobleaching; *es*, equilibrative sensitive; *ei*, equilibrative insensitive; MTT, 3-(4,5-dimethylthiazol-2-yl)-5-(3-carboxymethoxyphenyl)-2-(4-sulfophenyl)-2*H*-tetrazolium; PBS, phosphate-buffered saline; $t_{1/2}$, half-recovery time; Urd, uridine; FuPmR, 3-(β-D-ribofuranosyl)furo[2,3-*d*]pyrimidin-2(3*H*)-one; dFuPmR, 3-(2-deoxy-β-D-*erythro*-pentofuranosyl)furo[2,3-*d*]-pyrimidin-2(3*H*)-one.

10.1021/bi0520535 CCC: $33.50
Published on Web 01/07/2006

hENT1 and -2 are functionally distinguished by different sensitivities (hENT1 ≫ hENT2) to nitrobenzylmercaptopurine ribonucleoside (NBMPR) and have therefore been assigned the functional designations equilibrative sensitive (*es*) and equilibrative insensitive (*ei*), respectively (*3*, *4*). hENT3, which is proton-dependent and, like hENT1, broadly selective, transports nucleosides across lysosomal membranes (*5*−*7*), and hENT4, which mediates equilibrative transport of adenosine (*5*, *8*), also transports monoamine neurotransmitters (*9*). The three hCNTs differ functionally in their permeant selectivities (*10*−*12*). hCNT1 and -2 prefer pyrimidine nucleosides and purine nucleosides, respectively, although hCNT1 also transports adenosine and hCNT2 also transports uridine (Urd), whereas hCNT3 transports both pyrimidine and purine nucleosides.

Interest in nucleoside transporters has increased because of their potential and proven therapeutic applications in cancer, stroke, and cardiovascular, parasitic, and viral diseases. Nucleoside transporter proteins are critical in controlling extracellular concentrations of adenosine, the ligand for cell-surface purinergic P1 receptors, which are involved in a variety of physiological responses, including coronary vasodilation, neuromodulation, and platelet aggregation (*13*, *14*). Nucleoside analogue chemotherapy is increasingly important in the therapy of many hematological as well as solid malignancies. The presence of nucleoside transporters in plasma membranes is required for efficient delivery of many anti-cancer nucleoside drugs (e.g., gemcitabine, capecitabine, and fludarabine) and has been linked mechanistically with drug sensitivities and toxicities (*15*−*17*). Several studies have demonstrated that deficiency of hENT1, the most widely abundant and distributed nucleoside transporter in human cells, confers resistance to cytotoxic nucleoside drugs (*18*−*22*). Studies on four cultured human pancreatic cancer lines (*23*) showed that hENT1 was the major transporter responsible for uptake of gemcitabine, the only approved pyrimidine nucleoside analogue for pancreatic cancer chemotherapy. A recent retrospective study showed that patients with pancreatic adenocarcinoma with high levels of detectable hENT1 protein had a significantly longer survival after gemcitabine treatment than patients with tumors with low levels or without detectable hENT1 (*24*), consistent with the hypothesis that hENT1-mediated nucleoside transport is a determinant of response to nucleoside drugs in some cancers. Development of predictive assays that can quickly determine the nucleoside transportability of cancer cells should mitigate resistance to nucleoside chemotherapy.

The presence of *es* and *ei* activities has been demonstrated in preparations containing nuclear envelope and endoplasmic reticulum membranes, suggesting that hENT1 and hENT2 may mediate translocation of nucleosides between intracellular compartments (*25*). hENT1 has been detected in mitochondrial membranes and may be involved in mitochondrial toxicity caused by some antiviral nucleosides (*26*). The newly identified hENT3 was found to be partially localized in lysosomal membranes (*25*) and may play a role in lysosomal release of nucleosides derived from degradation of nuclear nucleic acids. However, knowledge of intracellular trafficking and distribution of nucleosides and nucleoside metabolites is limited.

Several fluorescent nucleoside analogues have been developed for the analysis of DNA and RNA structures. These

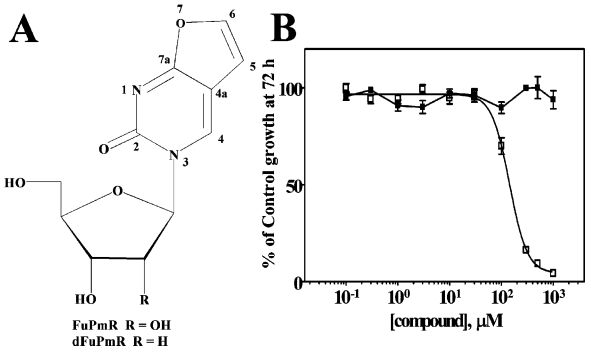

FIGURE 1: Structures and cytotoxicities of FuPmR and dFuPmR. (A) Chemical structures of 3-(β-D-ribofuranosyl)furo[2,3-*d*]pyrimidin-2(3*H*)-one (FuPmR) and 3-(2-deoxy-β-D-*erythro*-pentofuranosyl)furo[2,3-*d*]pyrimidin-2(3*H*)-one (dFuPmR). (B) Growth-inhibitory effects of FuPmR and dFuPmR on BeWo cells. Actively proliferating cells were incubated at 37 °C with graded concentrations of FuPmR (open squares) or dFuPmR (closed squares) for 72 h, after which the MTT assay was conducted as described in Materials and Methods. Representative cytotoxicity relationships are shown; each data point represents the mean ± SE of six determinations, and error bars are not shown where they are smaller than the symbol. IC_{50} values (given in the text) were obtained from the MTT−cytotoxicity relationships (means of at least three independent experiments).

analogues (e.g., a cytidine analogue pyrrolo-dC, 5′-dimethoxytrityl-[6-methyl-pyrrolo-[2,3-*d*]-pyrimidine-2(3*H*)-one]-2′-deoxyribonucleoside, 3′-[(2-cyanoethyl)-(*N*,*N*-diisopropyl)]) are prepared as phosphoramidites and used for in vitro DNA labeling with commercial DNA polymerases (*27*), suggesting that they are not permeants of nucleoside transporters. The fluorescence signal measurements are usually carried out with a fluorimeter. We describe here the development of a novel strategy for visualizing and measuring transport processes in living cells. FuPmR [3-(β-D-ribofuranosyl)furo[2,3-*d*]-pyrimidin-2(3*H*)-one] and dFuPmR [3-(2-deoxy-β-D-*erythro*-pentofuranosyl)furo[2,3-*d*]pyrimidin-2(3*H*)-one] were assessed as prototypic fluorescent nucleoside probes (see Figure 1A for chemical structures). The transportabilities of FuPmR and dFuPmR by hENT1 and -2 were assessed by live cell imaging in cultured human BeWo choriocarcinoma cells, which possess high levels of *es* activity (i.e., hENT1). Inhibition of cellular uptake by potent and specific inhibitors of hENT1-mediated transport demonstrated involvement of hENT1 in passage across plasma membranes. Quantitative live cell imaging analysis demonstrated different initial rates of FuPmR uptake by 10 other human cancer cell lines with various levels of nucleoside transport activity, suggesting a potential role of FuPmR transportability in assessing hENT1 abundance. The movements of FuPmR across various membranes were further confirmed by fluorescence recovery after photobleaching (FRAP). The measurement of cellular and organellar uptake of fluorescent nucleoside analogues by fluorescence microscopy with digital processing of data to extract rates provides a new approach to quantitatively study nucleoside transport activities and to evaluate the intracellular distribution of nucleosides and their metabolites in living cells.

The new approach described in the current study for analysis of intracellular events involving nucleosides and/or nucleoside metabolites will enable real-time studies of trafficking of nucleosides and their metabolites. Development

of autofluorescent permeants for other types of transporters will open a new avenue within the transporter research field.

MATERIALS AND METHODS

Synthesis of FuPmR and dFuPmR. The fluorescent furopyrimidine analogues were synthesized by the methods of Robins and Barr (*28*, *29*). Briefly, 2′,3′,5′-tri-*O*-acetyluridine (for FuPmR) and 3′,5′-di-*O*-acetyl-2′-deoxyuridine (for dFuPmR) were iodinated (*28*), and the 5-iodo compounds were coupled with trimethylsilylacetylene (*29*). Fluoride-promoted removal of the trimethylsilyl group followed by copper(I) iodide-catalyzed cyclization gave the furopyrimidine derivatives (*29*), which were deacylated with methanolic ammonia to provide 3-(β-D-ribofuranosyl)furo[2,3-*d*]pyrimidin-2(3*H*)-one (FuPmR) and 3-(2-deoxy-β-D-*erythro*-pentofuranosyl)-furo[2,3-*d*]pyrimidin-2(3*H*)-one (*30*) (dFuPmR). The structures of FuPmR and dFuPmR are shown in Figure 1A.

Cell Culture and Cytotoxicity Assays. The origins and maintenance of human choriocarcinoma (BeWo) cells were described previously (*31*). Human cell lines, which were obtained from American Type Culture Collection (ATCC, Manassas, VA), were breast cancer cell lines MCF-7 (estrogen receptor positive) and MDA-MB-231 (estrogen receptor negative), pancreatic cancer cell lines CaPan and MIA PaCa-2, ovarian cancer cell lines OVCAR-3 and SKOV-3, lung cancer cell lines A498 and A594, glioblastoma cell line U251, and cervical cancer cell line HeLa. Cells were grown as adherent monolayers in Roswell Park Memorial Institute 1640 medium supplemented with 10% fetal bovine serum (v/v) at 37 °C in 5% CO_2/95% air and were subcultured by trypsinization every 2−3 days to maintain exponential growth. Two days before imaging experiments, cells were seeded into a 6-well plate, each well of which contained a glass coverslip (5000 cells/well in 2 mL of growth medium).

Cytotoxicity assays were conducted with the CellTiter 96 proliferation assay kit (Promega, Madison, WI). Cells were seeded into 96-well plates at densities of 5000 (72-h exposures) or 20 000 cells (4-h exposures) per well and incubated at 37 °C for 24 h before exposure to test compounds. Cells were exposed to graded concentrations of FuPmR or dFuPmR (0−1000 μM) for 4 or 72 h and then treated with 3-(4,5-dimethylthiazol-2-yl)-5-(3-carboxymethoxyphenyl)-2-(4-sulfophenyl)-2*H*-tetrazolium (MTT) reagent for assessment of cytotoxicity as described by the manufacturer. The concentrations that reduced MTT-dependent absorbance by 50% (IC_{50} values) were calculated from nonlinear regression analysis of data plotted as percentages of control values against the logarithm of the fluorescent analogue concentrations.

Measurement of [^{3}H]Urd Uptake Mediated by Recombinant NTs Produced in Saccharomyces cerevisiae. Construction of the yeast expression systems for hENT1 and -2 and hCNT1, -2, and -3 was performed as described (*32*−*34*). Yeast producing individual recombinant hENT or hCNT proteins were maintained in logarithmic growth phase in complete minimal medium (pH 7.4) with 2% glucose. Transport experiments were conducted with a high-throughput assay described previously (*33*) that used 96-well plates and a semiautomated cell harvester (Micro96 Harvester; Skatron Instruments, Lier, Norway). The relative affinities of the transporters for FuPmR and dFuPmR were assessed by measuring the concentration dependence of their inhibition of uptake of [^{3}H]Urd as follows. Yeast producing recombinant hENT1, hENT2, hCNT1, hCNT2, or hCNT3 were incubated with graded concentrations of FuPmR and dFuPmR in the presence of 1 μM [^{3}H]Urd for 10 min (hENT1, -2 and hCNT1, -2) or 5 min (hCNT3). Each experiment was repeated at least three times. Nonspecifically associated radioactivity was determined in the presence of 10 mM nonradioactive Urd, and the resulting values were subtracted from total uptake values. Data were subjected to nonlinear regression analysis using GraphPad Prism Software version 3.0 (GraphPad Software Inc., San Diego, CA) to obtain IC_{50} values for FuPmR and dFuPmR; K_i values were determined using the Cheng−Prusoff equation (*35*) and the K_m values for transport of Urd obtained for each of the recombinant transporters produced in yeast (*33*, *34*, *36*).

Production of Recombinant hCNTs and Measurement of hCNT-Induced Sodium and Proton Currents in Oocytes of Xenopus laevis. The cDNAs of hCNT1, -2, and -3 were individually subcloned into vector pGEM-HE. Plasmids were linearized with *Nhe*I (pGEM-HE) and transcribed with T7 polymerase mMESSAGE mMACHINE (Ambion Inc., Austin, TX). Stage VI oocytes of *X. laevis* were microinjected with 20 nL of water or 20 nL of water containing RNA transcripts (20 ng) for the appropriate transporter and incubated in modified Barth's medium (changed daily) at 18 °C for 72 h as described (*37*) prior to the assay of transport activity.

Oocyte membrane currents were measured using a GeneClamp 500Boocyte clamp (Axon Instruments, Inc., Foster City, CA) in the two-electrode, voltage-clamp mode as described (*37*). All experiments were performed at room temperature (20 °C), and oocytes were discarded if the membrane potential was unstable or more positive than −30 mV. Membrane potentials were clamped at a holding potential (V_h) of −50 mV. Oocytes were perfused with transport medium containing 100 mM NaCl, 2 mM KCl, 1 mM $CaCl_2$, 1 mM $MgCl_2$, and 10 mM HEPES, pH 7.5 or 8.5, and cation/nucleoside cotransport was initiated by changing the permeant-free solution to one containing 100 μM Urd, dFuPmR, or FuPmR. For experiments that were conducted in the absence of sodium, choline replaced sodium, and proton-dependent uptake of Urd, dFuPmR, or FuPmR was measured in choline-containing transport medium acidified to pH 5.5 (buffered with 10 mM MES) (*37*).

NBMPR Binding by Intact Adherent Cells. Cells (50 000/well) were seeded in 12-well cell culture plates and maintained for 2 days before the binding experiments. Site-specific binding of [^{3}H]NBMPR (Moravek Biochemicals, Brea, CA) was determined at room temperature using replicate adherent cultures (5 per assay) as described previously (*38*). The mean number of cells per well for each plate was determined by counting cells in each of two wells. Cultures were cooled to room temperature, rinsed with sodium buffer (130 mM NaCl, 3 mM K_2HPO_4, 2 mM $CaCl_2$, 1 mM $MgCl_2$, 20 mM Tris/HCl, and 5 mM glucose, pH 7.4), and incubated with a saturating concentration (5 nM) of [^{3}H]NBMPR (500 μL/well in sodium buffer) in the absence or, to determine nonspecific binding, in the presence of 10 μM nonradioactive NBMPR. Cells were incubated for 60 min, and the binding assays were ended by removing the

media by aspiration, followed by rinsing with 2 mL of sodium buffer. The air-dried cells were solubilized by treatment with 500 μL 0.5 M NaOH for 60 min, and the cell-associated radioactivities in the resulting solvent were determined by liquid-scintillation counting. Specifically bound NBMPR was determined by subtracting values associated with cells in the presence of 10 μM nonradioactive NBMPR from values associated with cells in its absence. Results were expressed as NBMPR binding sites per cell.

Time-Lapse Confocal Microscopy and Fluorescence Recovery after Photobleaching. Time-lapse microscopy was performed using a Zeiss LSM510 Confocal Laser Scanning Microscope (Carl Zeiss, Jena, Germany) mounted on an Axiovert 100M inverted microscope. A coverslip with adhered BeWo cells was washed three times with phosphate-buffered saline (PBS, pH 7.4) and glued onto the edge of an open hole located in the middle of a 2-μm thick metal slide to form a well. Five hundred microliters of PBS alone or PBS containing the appropriate transport inhibitor at the desired concentration was added to the well, which was held at room temperature for 5 min before confocal studies. The solution in the well was maximally removed by gentle suction, and time-lapse image capturing was started a few seconds before adding 500 μL of PBS containing the appropriate autofluorescent nucleoside analogue into the well. The live cell imaging lasted 10−70 min. To visualize mitochondria, cells growing on glass coverslips were incubated with 0.1 μM MitoTracker Orange (Molecular Probes, Inc., Eugene, OR) in cell culture medium for 30 min at 37 °C in the dark in an atmosphere of 5% CO_2, washed three times with PBS, and subjected to confocal imaging. Time-lapse images were collected with 40× (NA1.3) F-fluar lenses and digitized at 12 bits with an interval of 1−3 s during the first 5 min and 60 s after 5 min. The zoom and frame sizes were set according to the Nyquist digitization criteria. Minimum laser intensities were used to collect the images to reduce the photobleaching and phototoxicity to the cells. For FuPmR and dFuPmR, a 351-nm laser line was used as the excitation source, and the emission signal was collected with a Longpass filter of 385 nm. For Mitotracker Orange, an excitation of 543 nm laser line was used and the emission signal was collected with a Longpass filter of 560 nm.

Fluorescence recovery after photobleaching (FRAP) analyses were performed using the same microscope. Photobleaching of the fluorescent signal at the focal plane of interest was performed using wavelengths of 351 and 364 nm at maximum power for 10 iterations. Time-lapse images were collected immediately before and after photobleaching. Differential interference contrast (DIC) images of cells were taken before and after FRAP in case there were changes in cell shape and position; none were observed. Average $t_{1/2}$, the time for fluorescence to recover to 50% of its original value, was determined from fluorescence recovery curves that were generated by plotting change in fluorescence intensity of a whole cell as a function of time.

Fluorescence intensities were measured by placing a circle around the stored digital image of a targeted cell or intracellular part. The integrated intensities were exported to a linked Microsoft Excel worksheet. Background fluorescence, which was defined as the fluorescent intensity of the same measurement circle in a nearby extracellular region, was determined and subtracted from each cellular measurement.

RESULTS

Cytotoxicity of FuPmR and dFuPmR to BeWo Cells. Previous studies showed that BeWo cells possess *es*- and *ei*-mediated nucleoside transport activities and extraordinarily high NBMPR-binding sites (*38*) and express hENT1 and hENT2 mRNAs (*25*). Before using FuPmR and DFuPmR in live cell imaging studies, we assessed their toxicities to BeWo cells during short (4 h) and prolonged (72 h) exposure periods using the MTT cytotoxicity assay. The 4-h exposures to either compound had no effect (data not shown), whereas the 72-h exposures revealed differences in cytotoxicity at high concentrations. At 1 mM, <5% of the cells survived FuPmR exposures, whereas >90% of the cells survived dFuPmR exposures; FuPmR had an IC_{50} (inhibitory concentration 50%) value of 146 ± 10 μM (Figure 1B). All subsequent experiments involved exposures of <1.1 h.

Interaction of FuPmR and dFuPmR with Recombinant Nucleoside Transporters Produced in Yeast. The inhibitory effects of FuPmR and dFuPmR on transporter-mediated uptake of [^{3}H]Urd was examined using a yeast expression system as previously described (*32*−*34*). Representative concentration−effect curves for FuPmR and dFuPmR inhibition of hENT1-, hENT2-, hCNT1-, hCNT2-, and hCNT3-mediated Urd transport are shown in Figure 2. The IC_{50} values obtained from the data of Figure 2 and previously reported kinetic constants for Urd (*33*, *34*, *39*) were used to calculate apparent K_i values, which provided a measure of the relative affinities of FuPmR and dFuPmR for the various transporters. hCNT3 displayed relatively high affinities for FuPmR and dFuPmR, with apparent K_i values (mean ± SE, $n = 3$) of 4.2 ± 0.8 and 15 ± 2 μM, respectively. FuPmR and dFuPmR were moderate inhibitors of hENT1-mediated Urd transport, with apparent K_i values (mean ± SE, $n = 3$) of 380 ± 20 and 170 ± 11 μM, respectively. Although hCNT1-mediated transport of Urd was sensitive to inhibition by both compounds, high concentrations did not completely inhibit transport, and apparent K_i values could not be calculated. FuPmR and dFuPmR were poor inhibitors of Urd uptake mediated by either hENT2 or hCNT2, with maximum inhibitory effects (50−70%) observed at concentrations of 3 mM.

Transportability of FuPmR and dFuPmR by hCNT1, hCNT2, and hCNT3 Produced in X. laevis Oocytes. The transportability of FuPmR and dFuPmR by members of the hCNT protein family was examined by comparing the currents they induced in *X. laevis* oocytes producing recombinant hCNT1, -2, or -3. Figure 3A shows representative total current recordings in hCNT-producing oocytes bathed in 100 mM Na^+-containing transport medium at pH 8.5 (to minimize proton-coupled transport) or 100 mM ChCl Na^+-free medium at pH values of 7.5 and 5.5. Urd, which was included at 100 μM as a control permeant, elicited large currents in Na^+-containing medium for all three transporters and in choline-containing medium at pH 5.5 for hCNT3. No currents were detected in control oocytes that had been injected with water without transporter transcripts.

For hCNT1-producing oocytes, small inward currents were elicited by application of 100 μM FuPmR or dFuPmR with

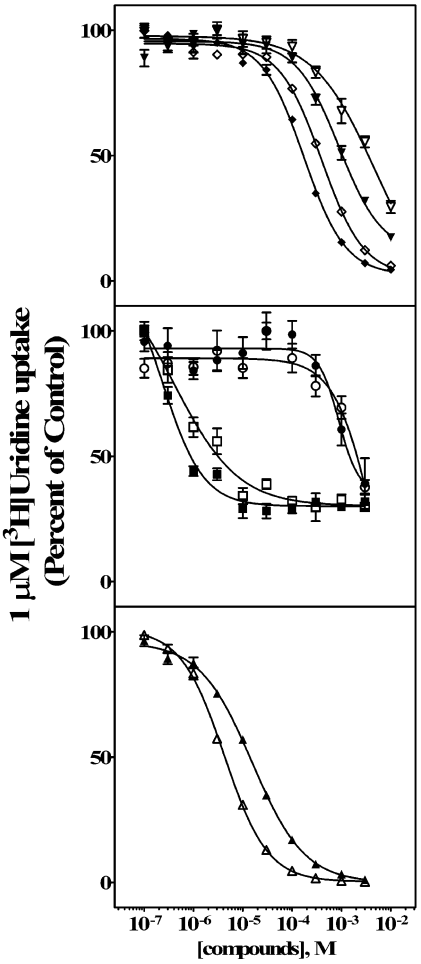

FIGURE 2: Inhibition of Urd uptake in yeast producing recombinant human nucleoside transporters by FuPmR or dFuPmR. The uptake of 1 μM [^{3}H]Urd into yeast producing the appropriate recombinant human nucleoside transporter was measured at room temperature over 20 min (hENT1 and -2, hCNT1 and -2) or 5 min (hCNT3) in the presence or absence of graded concentrations of FuPmR (open symbols) or dFuPmR (closed symbols) as described in Material and Methods. The nucleoside transporters were hENT1 (◆, ◇), hENT2 (▼, ▽), hCNT1 (■, □), hCNT2 (●, ○), and hCNT3 (▲, △). Uptake values in the presence of FuPmR or dFuPmR are given as the percentage of uptake values in their absence. Each data point represents the mean ± SE of quadruplicate determinations; error bars are not shown where they are smaller than the symbol. Results from representative experiments are shown; three or four independent experiments gave similar results.

slightly higher currents (mean ± SE, $n = 3$) observed with FuPmR ($I_{Na} = 11 \pm 0.9$ nA) than with dFuPmR ($I_{Na} = 6.5 \pm 0.3$ nA). For hCNT2-producing oocytes, no currents were elicited by either 100 μM FuPmR or dFuPmR. No currents were observed with 100 μM Urd, FuPmR, or dFuPmR when oocytes producing recombinant hCNT1 or hCNT2 were perfused with sodium-free ChCl medium at pH 7.5 or 5.5 (Figure 3B).

hCNT3 has a greater ability to transport permeants against their concentration gradients than either hCNT1 or -2, because its sodium/nucleoside coupling ratio is 2:1, whereas that of hCNT1 and -2 is 1:1 (*40*). Additionally, hCNT3 differs from hCNT1 and -2 in that it is also proton-dependent (*40*). Both sodium and proton currents were observed in oocytes producing hCNT3 (Figure 3). Large sodium-dependent currents (mean ± SE, $n = 3$) were induced by 100 μM Urd (140 ± 15 nA), FuPmR (77 ± 8 nA), and dFuPmR (89 ± 11 nA) at pH 8.5. When choline was used as the sodium substitute, a small current was observed with 100 μM Urd at pH 7.5, whereas no current was observed with either 100 μM FuPmR or dFuPmR. In acidified choline-containing medium (pH 5.5), small but reproducible proton currents (mean ± SE, $n = 3$) were produced by application of 100 μM FuPmR (13 ± 2 nA) or dFuPmR (3.5 ± 1.5 nA).

Live Cell Imaging of FuPmR Uptake into BeWo Cells. The uptake of FuPmR into BeWo cells was evaluated using confocal microscopy and an excitation wavelength of 351 nm. Autofluorescence of BeWo cells was observed (Figure 4A, time 0 s). The extracellular medium emitted fluorescence (color-coded as green) instantly upon addition of 500 μM FuPmR to the well whose bottom was the coverslip with BeWo cells attached (Figure 4A, time 0 s), and the fluorescent intensity of the medium barely changed during the observational period (Figure 4B). As shown in the time-lapse images of Figure 4A, the cytoplasm and the nucleus became fluorescent after exposure to FuPmR and a significant intracellular accumulation of fluorescent signals was observed by 15 min. The fluorescence intensities continued to increase over a period of 60 min (data not shown). The time course of intracellular fluorescence accumulation exhibited two phases of uptake (Figure 4B). The first phase lasted about 40 s with a steep slope, indicating a rapid initial rate of uptake. The second phase was slower, and the increase of intracellular fluorescence intensity was linear for about 1 h (data not shown), suggesting continuous trapping of FuPmR and/or its metabolites. No uptake of FuPmR was observed in the presence of 5 μM NBMPR (data not shown), indicating that FuPmR uptake was mediated primarily by hENT1. The uptake of FuPmR into other tested cell lines showed a similar two-phase phenomenon with varying time periods of the first phase (data not shown).

Mitotracker Orange was introduced as a control of the fluorescent signal as well as a probe for monitoring accumulation of FuPmR (and/or its metabolites) in mitochondria (Figure 4). The fluorescence intensities of Mitotracker orange maintained stable levels in intracellular compartments in the presence of 500 μM FuPmR (Figure 4B). Accumulation of FuPmR (and/or its metabolites) in mitochondria was evident since the green fluorescent signals of the mitochondrial compartment kept increasing (Figure 4A, combined channels) as shown by the gradual change of the fluorescent color from orange to yellow. A 3-fold increase of green fluorescent intensities was observed in mitochondrial regions in the presence of 500 μM FuPmR over 15 min (data not shown).

Experiments similar to those shown in Figure 4 were conducted in BeWo cells with the 2′-deoxy analogue dFuPmR (data not shown) and demonstrated uptake via an NBMPR-sensitive process (i.e., hENT1), albeit at slower rates than for FuPmR. Subsequent investigations were carried out exclusively with the riboside FuPmR.

Measuring Initial Rates of FuPmR Uptake. To calculate initial rates of FuPmR uptake during the first stage of cellular accumulation, which lasted for approximately 40 s, time zero was set at the moment of addition of FuPmR, and fluorescence intensity (after background subtraction) was normalized as the percentage of the highest uptake value (100%) during the initial 40-s exposure. The slopes of the uptake time courses were linear during the first few seconds and

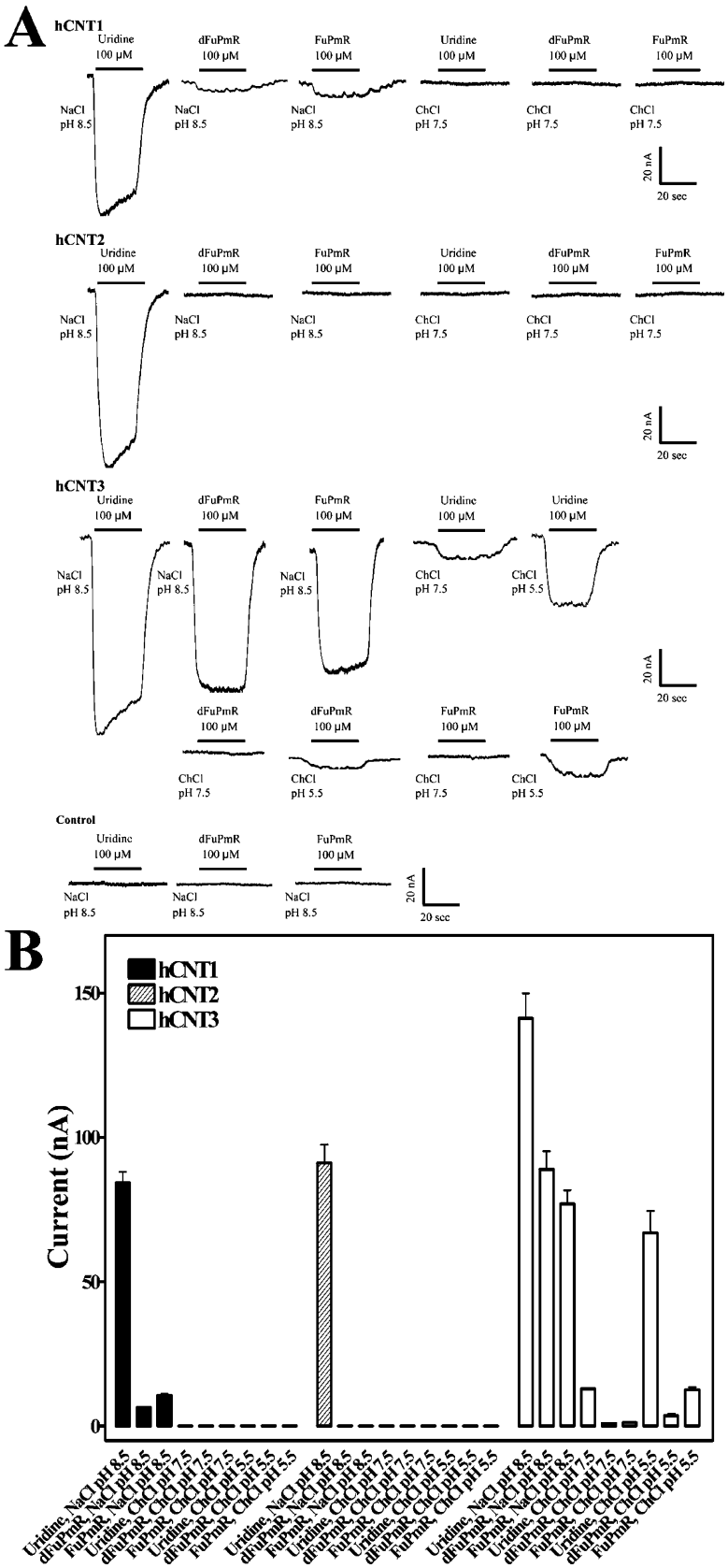

FIGURE 3: Analysis of transport of FuPmR and dFuPmR by hCNT1, -2, and -3. (A) Representative sodium and proton currents in the presence of FuPmR or dFuPmR. Oocytes were injected with 10 nL of water alone (control) or water that contained 20 ng of hCNT1, -2, or -3 transcripts as described in Materials and Methods. Currents were generated by perfusing individual oocytes producing either hCNT1, -2, or -3 with either 100 μM FuPmR or 100 μM dFuPmR in the appropriate transport mediums. The currents produced by 100 μM Urd in sodium-containing medium are shown for comparison. The same experiment was performed in a control water-injected oocyte (bottom panel). (B) Mean sodium and proton currents induced by Urd, FuPmR, and dFuPmR. Currents were generated as described for panel A in sodium-containing (pH 8.5) or sodium-free (pH 7.5 or pH 5.5) media. Values are means ± SE for three different oocytes. The same experiment was also performed in control water-injected oocytes (data not shown); no inward currents were generated.

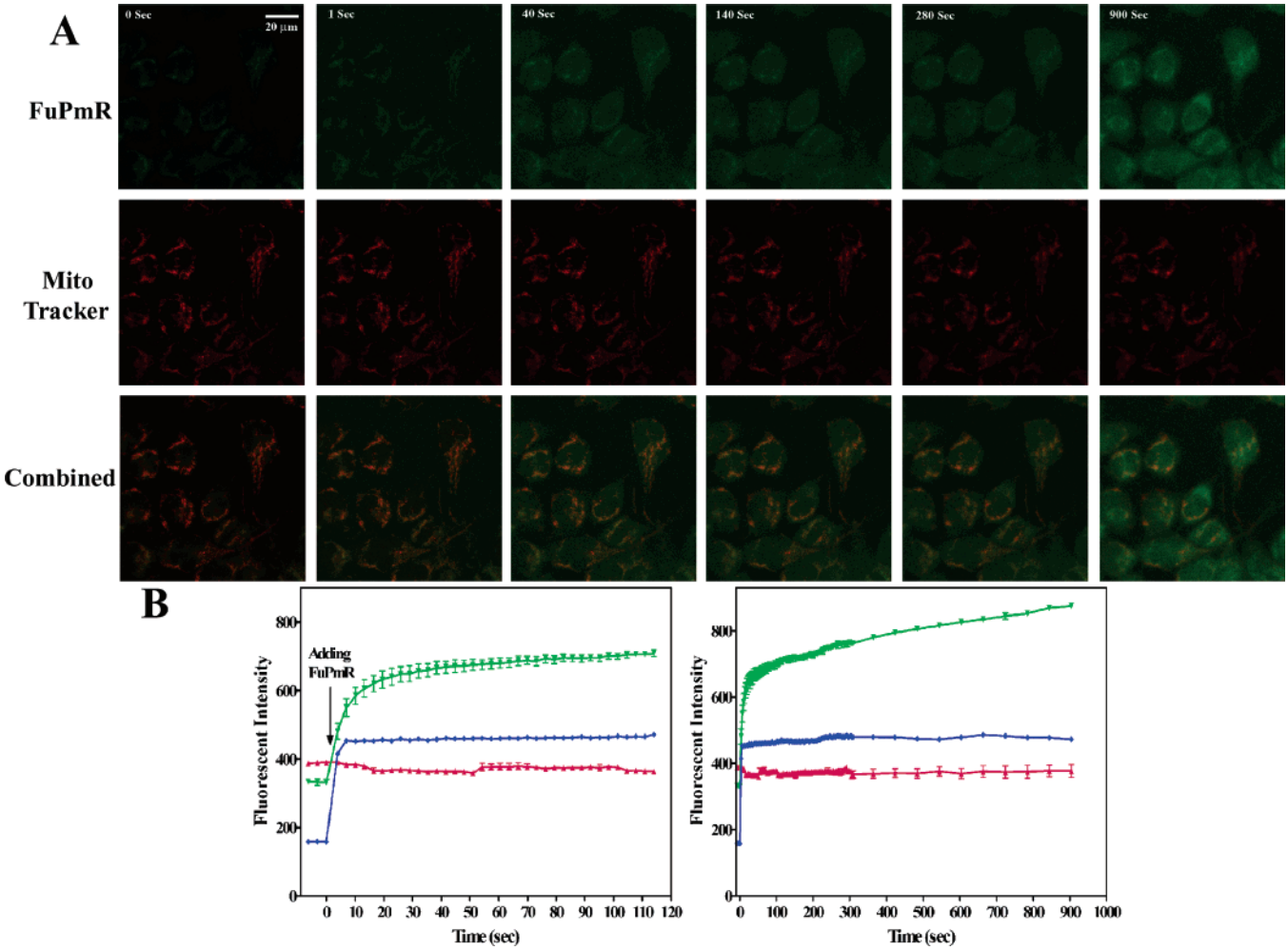

FIGURE 4: Live cell imaging of FuPmR uptake into BeWo cells. (A) Time-lapse series of images before and after the addition of FuPmR. BeWo cells were labeled with 0.1 μM MitoTracker Orange (shown in red channel) at 37 °C for 30 min, washed three times with PBS, and then incubated with 500 μM FuPmR (shown in green channel) for 1 h. Images were taken before adding FuPmR (first column) and every 3 s for the first 300 s and every 60 s until 1 h after the addition of FuPmR. Time in seconds is shown in the upper left corner. (B) Representative time courses of FuPmR uptake. The whole-cell fluorescence intensities of FuPmR (green line) and MitoTracker orange (red line) and the extracellular fluorescence intensities of FuPmR (blue line) at different time points were measured from eight cells and one extracellular region (similar in size as a cell), respectively, and the resulting mean values (± SE) were plotted against time. Each value for whole-cell fluorescence intensity is the mean ± SE of eight determinations, and SE values are not shown where they were smaller than the data points. The left graph shows the time courses for the first 120 s of the right graph.

yielded initial rates with mean values (± SE, $n = 5$ cells) of 9.3 ± 0.3 and 4.8 ± 0.2 (relative fluorescence intensity/cell)/s for 500 and 250 μM FuPmR, respectively (Figure 5B). Initial rates were greater at higher FuPmR concentrations, and saturated uptake rates were observed using 750 μM, 1 mM, or 2 mM FuPmR (Figure 5B,C, $n = 4-8$), indicating the concentration-dependence of uptake. The K_m value for FuPmR uptake was estimated (from visual inspection of rate versus concentration plots at the higher concentrations, data not shown) to be 300−400 μM, which was similar to the K_i value obtained in studies with recombinant hENT1 produced in yeast (Figure 2) and consistent with the conclusion that the transport of FuPmR into BeWo cells was mainly mediated by hENT1.

As shown in Figure 5A, a significant increase in fluorescence was observed in BeWo cells after a 5-min exposure to FuPmR, whereas little, if any, increase was observed in the presence of 5 μM NBMPR, indicating that permeation of FuPmR was mediated primarily by hENT1. Inhibition of FuPmR transport by NBMPR was concentration-dependent with an IC_{50} value of 1 nM (Figure 5C), which was close to values obtained with other nucleosides in radioisotope-flux experiments (*38*). The majority of FuPmR uptake was blocked by 10 or 100 nM NBMPR, and the remaining uptake was totally inhibited by 1 μM NBMPR. The NBMPR inhibitory experiment was also performed in sodium-free buffer, and similar results were observed, indicating that the uptake of FuPmR was mediated mostly by hENT1 and partially by hENT2, and no concentrative transport process of the fluorescent compound was observed in undifferentiated BeWo cells (data not shown). Two potent inhibitors of both hENT1 and -2, dipyridamole and dilazep, also inhibited FuPmR transport into BeWo cells (Figure 5C).

The rates of accumulation of FuPmR (500 μM) into different intracellular compartments were measured by placing circles of similar size on different parts of the digital time-lapse images of the same cells. The accumulation of FuPmR and/or its metabolites into organelles also followed a two-phase uptake pattern. However, the initial rates of uptake (mean ± SE, $n = 4$) into cytoplasmic regions (9.7 ±

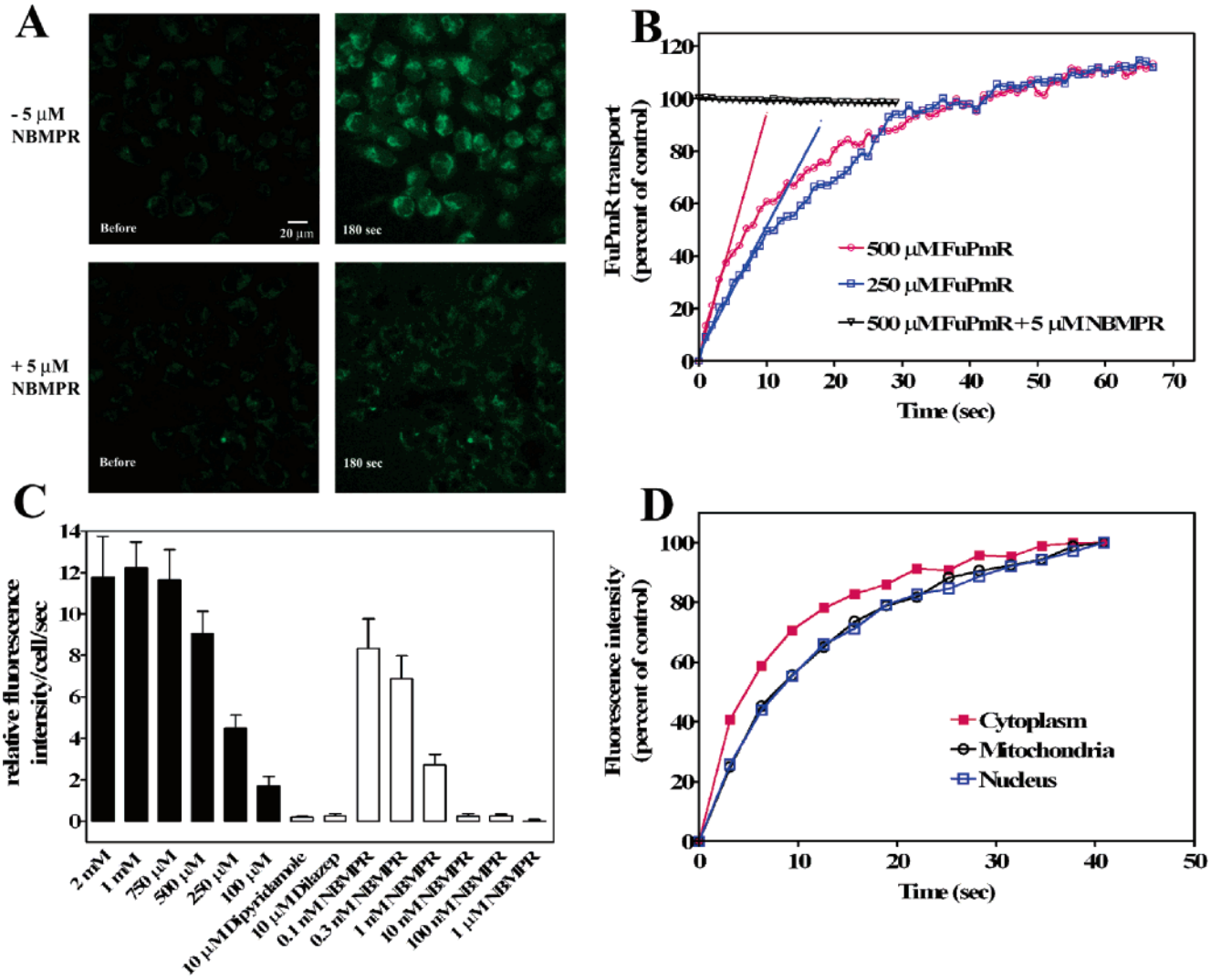

FIGURE 5: Use of live cell imaging to quantify rates of FuPmR transport into BeWo cells. (A) FuPmR accumulation into BeWo cells in the presence or absence of 5 μM NBMPR. Images were taken before and 180 s after the addition of 500 μM FuPmR to BeWo cells as described in Materials and Methods. (B) Representative time courses used to calculate initial rates of FuPmR uptake. To calculate the initial rates of FuPmR uptake, time zero was set at the point of adding 500 μL of either 250 or 500 μM FuPmR to the well, the bottom of which was a coverslip with adhered BeWo cells. Fluorescent intensities were measured and expressed as the percent of the highest uptake value (100%) during the first uptake stage. Values are means for four different determinations; SE values are not shown. (C) Effects of ENT inhibitors on initial rates of FuPmR uptake. The initial rates were calculated from time courses of uptake of various concentrations of FuPmR (closed bars) or 500 μM FuPmR together with either dipyridamole, dilazep, or NBMPR at the concentrations indicated (open bars). (D) Initial rates of fluorescent intensity changes in cytoplasmic, mitochondrial, and nuclear regions. Fluorescence intensities were measured in different regions of the same cell during exposure to 500 μM FuPmR, and initial rates were obtained as described in panel B. Values are means for three or four different determinations; SE values are not shown.

2.2 (relative fluorescence intensity/cell)/s) were slightly faster than those in mitochondrial and nuclear regions (8.0 $\pm$ 1.2 (relative fluorescence intensity/cell)/s) (Student's *t*-test, $p < 0.05$) (Figure 5D), suggesting that the passage of FuPmR (and/or its metabolites) across intracellular membranes also occurred by mediated processes.

Cellular uptake of the fluorescent nucleoside analogue was blocked at various time points using the hENT inhibitors (NBMPR, dipyridamole, and dilazep) to enable measurement of accumulation of the analogue into organellar compartments (data not shown). However, no measurable increase or decrease of fluorescence signals was observed. Possible explanations are that a concentration gradient was needed to maintain intercompartmental transport and/or that the fluorescent probe and the current experimental setup were not sensitive enough to measure minor changes in fluorescent signals.

Initial Rates of FuPmR Uptake and NBMPR Binding-Site Abundance. In humans, equilibrative nucleoside transport activity was detected in almost all cell types, and hENT1 appears to have a ubiquitous tissue distribution. Because the hENT1 abundance in cancer cells is a potential determinant of survival of patients treated with a nucleoside anticancer drug (*24*), we tested the hypothesis that the initial rate of FuPmR uptake reflects the abundance of hENT1 in cells. hENT1 abundance was determined by quantification of cellular NBMPR binding sites; numerous studies have established that high-affinity binding of NBMPR to human cells and tissues can be used to quantify hENT1 abundance (for review, see ref *1*). Table 1 summarizes results of

Table 1: The Abundance of NBMPR Binding Sites and the Initial Rates of FuPmR Uptake of 11 Human Cancer Cell Lines

cell lines	total NBMPR-binding sites per cell ($\times 10^5$) (mean ± SE)	initial rates of FuPmR uptake ((relative fluorescence intensity/cell)/s)		
		total	in the presence of 100 nM NBMPR	hENT1-mediated
BeWo	30.4 ± 1.8	9.1 ± 2.9	0.3 ± 0.1	8.8 ± 2.7
MDA-MB-231	5.9 ± 0.5	2.9 ± 0.3	ND[a]	2.9 ± 0.3
MIA PanCa-2	5.4 ± 0.3	3.2 ± 0.2	ND[a]	3.2 ± 0.2
MCF-7	3.6 ± 0.1	2.7 ± 0.2	1.2 ± 0.1	1.5 ± 0.2
SKOV-3	3.5 ± 0.4	2.1 ± 0.1	ND[a]	2.1 ± 0.1
A498	3.4 ± 0.1	2.0 ± 0.1	ND[a]	2.0 ± 0.1
HeLa	2.6 ± 0.2	2.3 ± 0.2	ND[a]	2.3 ± 0.2
A549	2.4 ± 0.2	1.3 ± 0.2	ND[a]	1.3 ± 0.2
U251	2.4 ± 0.1	1.6 ± 0.3	ND[a]	1.6 ± 0.3
OVCAR-3	1.8 ± 0.2	0.2 ± 0.03	ND[a]	0.2 ± 0.03
CaPan	1.4 ± 0.2	0.5 ± 0.1	0.4 ± 0.07	0.1 ± 0.04

[a] ND, not detectable.

NBMPR binding site studies in 11 human cell lines and the corresponding initial rates of 500 μM FuPmR uptake mediated by hENT1. Different values for the total number of NBMPR-binding sites were observed in the 11 cell lines (BeWo ≫ MDA-MB-231, MIA PaCa > MCF-7, SKOV-3, A498 > HeLa, A549, U251 > OVCAR-3, CaPan), indicating differences in the abundance of hENT1.

The approach illustrated in Figure 5B for BeWo cells was used to measure the initial uptake rates of FuPmR uptake during the first stage of cellular accumulation in the other cell lines. Similar results were observed for FuPmR uptake using PBS and sodium-free buffer, indicating that little FuPmR uptake, if any, was mediated by hCNTs. hENT1-mediated FuPmR uptake was represented by the difference of initial rates of 500 μM FuPmR uptake in the absence and presence of 100 nM NBMPR in sodium-free buffer (Table 1). For most cell lines, the vast majority of FuPmR uptake into cells was blocked by 100 nM NBMPR, and the remaining uptake was totally inhibited by 10 μM dilazep (data not shown).

The highest FuPmR uptake rates were observed in BeWo cells, which possess an unusually large number of NBMPR binding sites, as shown in the current and previous studies (*38*). Moderate initial rates of FuPmR uptake mediated by hENT1 (~3 (relative fluorescence intensity/cell)/s) were observed in MDA-MB-231 and MIA PaCa-2 cells with NBMPR-binding sites of about 5×10^5 per cell. Cells (MCF-7, SKOV-3, A498, HeLa, A549, and U251) with lower numbers of NBMPR binding sites exhibited reduced abilities to transport FuPmR with a hENT1-mediated uptake rate of 1−2 (relative fluorescence intensity/cell)/s. Dramatically low initial rates were observed in OVCAR-3 and CaPan cells, which also possessed low NBMPR-binding sites ($<2 \times 10^5$ per cell). These results suggested that the transportability of FuPmR, a hENT1 permeant, depends on and reflects the hENT1 abundance of cells.

FRAP Analysis of the Movement of the Fluorescent Compound. By photobleaching regions of whole cells that had been incubated with 500 μM FuPmR for 30 min, we determined the extent of recovery of fluorescence signals in whole cells by using FRAP. In the absence of 5 μM NBMPR, the bleached cells showed >50% recovery with a half-recovery time ($t_{1/2}$) of 80 s, whereas the nearby unbleached (control) cells exhibited continuous slow accumulation of fluorescence. The incomplete fluorescence recovery was partially due to the bleaching of autofluorescence, since the autofluorescence observed in cells without FuPmR treatment exhibited no recovery during the period of measurement (data not shown). In the presence of 5 μM NBMPR, recovery of fluorescence by bleached cells reached about 5% after 200 s, further evidence that the movement of FuPmR across plasma membranes was mediated by hENTs.

DISCUSSION

The most commonly used method to measure nucleoside transporter activities is analysis of radioisotope fluxes. Additionally, measurements of current can be used to assess activities of sodium and/or proton-coupled transporters. Approaches that could be used to visualize nucleoside transport activities in situ have not been available previously. Fluorescent inhibitors of ENT1 (e.g., SAENTA-χ_2-Fluorescein (*41*, *42*)) have enabled ligand−cell interactions to be analyzed by flow cytometry (*43*, *44*). We describe here a novel methodology for real-time visualization of nucleoside transport processes in living cells.

FuPmR and dFuPmR are autofluorescent nucleoside analogues that differ from each other by the presence of a hydroxyl group at the C(2′) position in FuPmR; they share high structural similarities with the naturally occurring pyrimidine nucleosides. An inhibitor sensitivity assay with yeast producing recombinant human nucleoside transporters revealed that both compounds were high-affinity inhibitors of hCNT3, moderate-affinity inhibitors of hENT1, and low-affinity inhibitors of hENT2, hCNT1, and hCNT2. Because hCNTs are cation/nucleoside cotransporters, the transportability of FuPmR and dFuPmR was tested by the voltage clamp technique, which showed that they were good and poor permeants for hCNT3 and hCNT1, respectively, and neither was transported by hCNT2. The transport of FuPmR and dFuPmR by hCNT1 and -3 both showed sodium-dependency and, in the case of hCNT3, proton-dependency, indicating a similar ion/permeant coupling mechanism for uptake of the fluorescent nucleoside probes as has been demonstrated for uridine and other naturally occurring nucleosides. The different affinities and transportability profiles for the nucleoside transporter subtypes raised the possibility that FuPmR and dFuPmR could be used as probes

to differentially detect nucleoside transport activities mediated by certain types of nucleoside transporters.

We used laser scanning confocal microscopy and the FRAP technique to demonstrate that transport processes could be directly visualized and quantified in situ with FuPmR. The fluorescent properties of FuPmR permitted assessment of hENT1 activity in BeWo cells, which exhibit large numbers ($>10^6$/cell) of NBMPR-binding sites and an unusually large capacity for NBMPR-sensitive nucleoside transport relative to other cell types (*38*). The uptake of FuPmR by BeWo cells was concentration-dependent with high sensitivity to nanomolar concentrations of NBMPR, indicating that its uptake was predominantly mediated by hENT1. Real-time imaging combined with fluorescence intensity digitalization revealed a two-stage uptake process. The first stage, which represented the true initial rate of the transport process, was short-lived. Previously, oil-stop and dilazep-stop methods (*45*), as well as a quenched-flow method (*46*), have been used to measure initial rates of nucleoside influx into mammalian cells. The second stage showed continued accumulation of fluorescent signals at much slower rates in a linear manner that lasted for at least an hour. The extended linear time courses may have resulted from intracellular metabolism of FuPmR (e.g., by phosphorylation), thereby maintaining the apparent concentration gradient of FuPmR between the extracellular and intracellular compartments. This live cell imaging approach was extended successfully to 10 other human cancer cell lines with different levels of hENT1 and demonstrated that FuPmR uptake rates reflected hENT1 abundance. The correspondence of FuPmR transportability to hENT1 abundance in live cells suggests that autofluorescent nucleoside analogues can be used as markers for rapid assessment of nucleoside transporter abundance.

Although *es* and/or *ei* transport activities have been observed in nuclear membranes, endoplasmic reticulum, and mitochondria (*25*, *26*) and endogenous hENT3 has been observed in the intracellular compartments of cells (*6*), the functional analyses of nucleoside transport processes across intracellular membranes has previously been conducted in isolated membrane preparations. The development of autofluorescent permeants offers the possibility of visualizing the intracellular distribution of nucleosides and/or their metabolites. Live cell imaging clearly showed accumulation of fluorescence into nuclei, which was further confirmed by FRAP experiments. The increased fluorescence intensities of mitochondrial regions after the application of FuPmR supplied the first in situ demonstration of movement of a nucleoside (or its metabolite) from cytosol to mitochondria. The initial rates of increase in fluorescence intensities in nuclear and mitochondrial regions were slower than those of a randomly selected cytoplasmic region of the same cell, suggesting that movement of FuPmR (or its metabolites) across nuclear and mitochondrial membranes was also mediated. It is known that nucleotides, the phosphorylated metabolites of nucleosides, must be transported across the highly impermeable inner mitochondrial membrane by specific transporters or translocators (*47*, *48*).

The properties of FuPmR raise the possibility that it could be used for other research purposes. For example, the availability of specific fluorescent permeants for nucleoside transporters would enable measurements of intracellular accumulation by flow cytometry, a technique that can differentiate subpopulations of cells on the basis of differences in fluorescence, allowing collection of high- or low-transport activity cells. Different nucleoside transporter subtypes have been localized on the apical and basolateral membranes of some polarized epithelia (*49*−*51*), and use of fluorescent nucleosides of which FuPmR is the prototype might enable visualization of trans-epithelial nucleoside transport in a cultured epithelium.

In conclusion, we have demonstrated that an autofluorescent nucleoside analogue can be used as a tool to visualize and quantify the transport process mediated by nucleoside transporters in living cells. FuPmR enabled visualization of the intracellular fate of a nucleoside (and/or its metabolite) in living cells for the first time. However, this analogue has limitations and must be regarded as the "proof of principle" prototype. The excitation peak of FuPmR is at 280 nm. UV excitation is not widely available for confocal laser scanning microscopy, and most optics for light microscopy have poor transmission in the UV range. More importantly, UV excitation is highly phototoxic to living cells, and excitation around 351 nm generates considerable autofluorescence from excitation of many biomolecules (e.g., NADH, NADHP, lipofuscin, nucleic acids, etc.). Ongoing efforts are focused on the design of highly sensitive fluorescent nucleoside probes with different excitation/emission spectra and unique permeant/inhibitor properties that will allow real-time, multicolor analysis of different nucleoside transporter subtypes in living cells.

REFERENCES

1. Cass, C. E. (1995) Nucleoside transport, in *Drug Transport in Antimicrobial and Anticancer Chemotherapy* (Georgopapadakou, N. H., Ed.) pp 403−451, Marcel Deker, New York.
2. Cass, C. E., Young, J. D., Baldwin, S. A., Cabrita, M. A., Graham, K. A., Griffiths, M., Jennings, L. L., Mackey, J. R., Ng, A. M. L., Ritzel, M. W. L., Vickers, M. F., and Yao, S. Y. M. (1999) Nucleoside transporters of mammalian cells, in *Membrane Transporters as Drug Targets* (Amidon, G. L., and Sadee, W., Eds.) pp 313−352, Kluwer Academic/Plenum Publishers, New York.
3. Edwards, A. M., Arrowsmith, C. H., Christendat, D., Dharamsi, A., Friesen, J. D., Greenblatt, J. F., and Vedadi, M. (2000) Protein production: feeding the crystallographers and NMR spectroscopists, *Nat. Struct. Biol. 7* (Suppl.), 970−972.
4. Coe, I. R., Griffiths, M., Young, J. D., Baldwin, S. A., and Cass, C. E. (1997) Assignment of the human equilibrative nucleoside transporter (hENT1) to 6p21.1-p21.2, *Genomics 45*, 459−460.
5. Acimovic, Y., and Coe, I. R. (2002) Molecular evolution of the equilibrative nucleoside transporter family: identification of novel family members in prokaryotes and eukaryotes, *Mol. Biol. Evol. 19*, 2199−2210.
6. Baldwin, S. A., Yao, S. Y., Hyde, R. J., Ng, A. M., Foppolo, S., Barnes, K., Ritzel, M. W., Cass, C. E., and Young, J. D. (2005) Functional characterization of novel human and mouse equilibrative nucleoside transporters (hENT3 and mENT3) located in intracellular membranes, *J. Biol. Chem. 280*, 15880−15887.
7. Hyde, R. J., Abidi, F., Griffiths, M., Yao, S. Y. M., Sundaram, M., Phillips, S. E. V., Cass, C. E., and Young, J. D. (2000) Probing the structure/function relationships of human equilibrative nucleoside transporters using site-directed mutagenesis, *Drug Dev. Res. 50*, 38.
8. Baldwin, S. A., Beal, P. R., Yao, S. Y., King, A. E., Cass, C. E., and Young, J. D. (2004) The equilibrative nucleoside transporter family, SLC29, *Pfluegers Arch. 447*, 735−743.
9. Engel, K., Zhou, M., and Wang, J. (2004) Identification and characterization of a novel monoamine transporter in the human brain, *J. Biol. Chem. 279*, 50042−50049.
10. Ritzel, M. W., Yao, S. Y., Huang, M. Y., Elliott, J. F., Cass, C. E., and Young, J. D. (1997) Molecular cloning and functional

expression of cDNAs encoding a human Na^+-nucleoside cotransporter (hCNT1), *Am. J. Physiol. 272*, C707−714.
11. Ritzel, M. W., Yao, S. Y., Ng, A. M., Mackey, J. R., Cass, C. E., and Young, J. D. (1998) Molecular cloning, functional expression and chromosomal localization of a cDNA encoding a human Na^+/nucleoside cotransporter (hCNT2) selective for purine nucleosides and uridine, *Mol. Membr. Biol. 15*, 203−211.
12. Ritzel, M. W. L., Ng, A. M., Yao, S. Y. M., Graham, K., Loewen, S. K., Smith, K. M., Ritzel, R. G., Mowles, D. A., Carpenter, P., Chen, X., Karpinski, E., Hyde, R. J., Baldwin, S. A., Cass, C. E., and Young, J. D. (2001) Molecular identification and characterization of novel human and mouse concentrative Na^+-nucleoside cotransporter proteins (hCNT3 and mCNT3) broadly selective for purine and pyrimidine nucleosides (system *cib*), *J. Biol. Chem. 276*, 2914−2927.
13. Van Belle, H. (1993) Nucleoside transport inhibition: a therapeutic approach to cardioprotection via adenosine?, *Cardiovasc. Res. 27*, 68−76.
14. Baldwin, S. A., Mackey, J. R., Cass, C. E., and Young, J. D. (1999) Nucleoside transporters: molecular biology and implications for therapeutic development, *Mol. Med. Today 5*, 216−224.
15. Mackey, J. R., Jennings, L. L., Clarke, M. L., Santos, C. L., Dabbagh, L., Vsianska, M., Koski, S. L., Coupland, R. W., Baldwin, S. A., Young, J. D., and Cass, C. E. (2002) Immunohistochemical variation of human equilibrative nucleoside transporter 1 protein in primary breast cancers, *Clin. Cancer Res. 8*, 110−116.
16. Mackey, J. R., Galmarini, C. M., Graham, K. A., Joy, A. A., Delmer, A., Dabbagh, L., Glubrecht, D., Jewell, L. D., Lai, R., Lang, T., Hanson, J., Young, J. D., Merle-Beral, H., Binet, J. L., Cass, C. E., and Dumontet, C. (2005) Quantitative analysis of nucleoside transporter and metabolism gene expression in chronic lymphocytic leukemia (CLL): identification of fludarabine-sensitive and -insensitive populations, *Blood 105*, 767−774.
17. Mackey, J. R., Baldwin, S. A., Young, J. D., and Cass, C. E. (1998) Nucleoside transport and its significance for anticancer drug resistance, *Drug Resist. Updates 1*, 310−324.
18. Mackey, J. R., Mani, R. S., Selner, M., Mowles, D., Young, J. D., Belt, J. A., Crawford, C. R., and Cass, C. E. (1998) Functional nucleoside transporters are required for gemcitabine influx and manifestation of toxicity in cancer cell lines, *Cancer Res. 58*, 4349−4357.
19. Wiley, J. S., Taupin, J., Jamieson, G. P., Snook, M., Sawyer, W. H., and Finch, L. R. (1985) Cytosine arabinoside transport and metabolism in acute leukemias and T cell lymphoblastic lymphoma, *J. Clin. Invest. 75*, 632−642.
20. Gati, W. P., Paterson, A. R., Tyrrell, D. L., Cass, C. E., Moravek, J., and Robins, M. J. (1992) Nucleobase transporter-mediated permeation of 2′,3′-dideoxyguanosine in human erythrocytes and human T-lymphoblastoid CCRF-CEM cells, *J. Biol. Chem. 267*, 22272−22276.
21. Cass, C. E., King, K. M., Montano, J. T., and Janowska-Wieczorek, A. (1992) A comparison of the abilities of nitrobenzylthioinosine, dilazep, and dipyridamole to protect human hematopoietic cells from 7-deazaadenosine (tubercidin), *Cancer Res. 52*, 5879−5886.
22. Gati, W. P., Larratt, L. M., and Turner, A. R. (2001) Cellular abundance of *es* nucleoside transporters and differential drug toxicity in myelodysplastic syndrome (MDS) bone marrow cell subpopulations, *Proc. West. Pharmacol. Soc. 44*, 93−96.
23. Garcia-Manteiga, J., Molina-Arcas, M., Casado, F. J., Mazo, A., and Pastor-Anglada, M. (2003) Nucleoside transporter profiles in human pancreatic cancer cells: role of hCNT1 in 2′,2′-difluorodeoxycytidine-induced cytotoxicity, *Clin. Cancer Res. 9*, 5000−5008.
24. Spratlin, J., Sangha, R., Glubrecht, D., Dabbagh, L., Young, J. D., Dumontet, C., Cass, C., Lai, R., and Mackey, J. R. (2004) The absence of human equilibrative nucleoside transporter 1 is associated with reduced survival in patients with gemcitabine-treated pancreas adenocarcinoma, *Clin. Cancer Res. 10*, 6956−6961.
25. Mani, R. S., Hammond, J. R., Marjan, J. M., Graham, K. A., Young, J. D., Baldwin, S. A., and Cass, C. E. (1998) Demonstration of equilibrative nucleoside transporters (hENT1 and hENT2) in nuclear envelopes of cultured human choriocarcinoma (BeWo) cells by functional reconstitution in proteoliposomes, *J. Biol. Chem. 273*, 30818−30825.
26. Lai, Y., Tse, C. M., and Unadkat, J. D. (2004) Mitochondrial expression of the human equilibrative nucleoside transporter 1 (hENT1) results in enhanced mitochondrial toxicity of antiviral drugs, *J. Biol. Chem. 279*, 4490−4497.
27. Liu, C., and Martin, C. T. (2001) Fluorescence characterization of the transcription bubble in elongation complexes of T7 RNA polymerase, *J. Mol. Biol. 308*, 465−475.
28. Robins, M. J., Barr, P. J., and Giziewicz, J. (1982) Nucleic acid related compounds. 38. Smooth and high-yield iodination and chlorination at C-5 of uracil bases and *p*-toluyl-protected nucleosides, *Can. J. Chem. 60*, 554−557.
29. Robins, M. J., and Barr, P. J. (1983) Nucleic acid related compounds. 39. Efficient conversion of 5-iodo to 5-alkynyl and derived 5-substituted uracil bases and nucleosides, *J. Org. Chem. 48*, 1854−1862.
30. Woo, J., Meyer, R. B., Jr., and Gamper, H. B. (1996) G/C-modified oligodeoxynucleotides with selective complementarity: synthesis and hybridization properties, *Nucleic Acids Res. 24*, 2470−2475.
31. Pattillo, R. A., and Gey, G. O. (1968) The establishment of a cell line of human hormone-synthesizing trophoblastic cells in vitro, *Cancer Res. 28*, 1231−1236.
32. Visser, F., Vickers, M. F., Ng, A. M., Baldwin, S. A., Young, J. D., and Cass, C. E. (2002) Mutation of residue 33 of human equilibrative nucleoside transporters 1 and 2 alters sensitivity to inhibition of transport by dilazep and dipyridamole, *J. Biol. Chem. 277*, 395−401.
33. Zhang, J., Visser, F., Vickers, M. F., Lang, T., Robins, M. J., Nielsen, L. P., Nowak, I., Baldwin, S. A., Young, J. D., and Cass, C. E. (2003) Uridine binding motifs of human concentrative nucleoside transporters 1 and 3 produced in *Saccharomyces cerevisiae*, *Mol. Pharmacol. 64*, 1512−1520.
34. Zhang, J., Smith, K. M., Tackaberry, T., Visser, F., Robins, M. J., Nielsen, L. P., Nowak, I., Baldwin, S. A., Young, J. D., and Cass, C. E. (2005) Uridine binding and transportability determinants of human concentrative nucleoside transporters, *Mol. Pharmacol. 68*, 830−839.
35. Cheng, Y., and Prusoff, W. H. (1973) Relationship between the inhibition constant (K_i) and the concentration of inhibitor which causes 50% inhibition (IC_{50}) of an enzymatic reaction, *Biochem. Pharmacol. 22*, 3099−3108.
36. Visser, F., Baldwin, S. A., Isaac, R. E., Young, J. D., and Cass, C. E. (2005) Identification and mutational analysis of amino acid residues involved in dipyridamole interactions with human and *Caenorhabditis elegans* equilibrative nucleoside transporters, *J. Biol. Chem. 280*, 11025−11034.
37. Smith, K. M., Ng, A. M., Yao, S. Y., Labedz, K. A., Knaus, E. E., Wiebe, L. I., Cass, C. E., Baldwin, S. A., Chen, X. Z., Karpinski, E., and Young, J. D. (2004) Electrophysiological characterization of a recombinant human Na^+-coupled nucleoside transporter (hCNT1) produced in *Xenopus* oocytes, *J. Physiol. 558*, 807−823.
38. Boumah, C. E., Hogue, D. L., and Cass, C. E. (1992) Expression of high levels of nitrobenzylthioinosine-sensitive nucleoside transport in cultured human choriocarcinoma (BeWo) cells, *Biochem. J. 288*, 987−996.
39. Visser, F., Zhang, J., Raborn, R. T., Baldwin, S. A., Young, J. D., and Cass, C. E. (2005) Residue 33 of human equilibrative nucleoside transporter 2 is a functionally important component of both the dipyridamole and nucleoside binding sites, *Mol. Pharmacol. 67*, 1291−1298.
40. Hamilton, S. R., Yao, S. Y., Ingram, J. C., Hadden, D. A., Ritzel, M. W., Gallagher, M. P., Henderson, P. J., Cass, C. E., Young, J. D., and Baldwin, S. A. (2001) Subcellular distribution and membrane topology of the mammalian concentrative Na^+-nucleoside cotransporter rCNT1, *J. Biol. Chem. 276*, 27981−27988.
41. Jamieson, G. P., Brocklebank, A. M., Snook, M. B., Sawyer, W. H., Buolamwini, J. K., Paterson, A. R., and Wiley, J. S. (1993) Flow cytometric quantitation of nucleoside transporter sites on human leukemic cells, *Cytometry 14*, 32−38.
42. Wiley, J. S., Brocklebank, A. M., Snook, M. B., Jamieson, G. P., Sawyer, W. H., Craik, J. D., Cass, C. E., Robins, M. J., McAdam, D. P., and Paterson, A. R. (1991) A new fluorescent probe for the equilibrative inhibitor-sensitive nucleoside transporter. 5′-S-(2-aminoethyl)-N6-(4-nitrobenzyl)-5′-thioadenosine (SAENTA)-chi 2-fluorescein, *Biochem. J. 273*, 667−672.
43. Sen, R. P., Delicado, E. G., Alvarez, A., Brocklebank, A. M., Wiley, J. S., and Miras-Portugal, M. T. (1998) Flow cytometric studies of nucleoside transport regulation in single chromaffin cells, *FEBS Lett. 422*, 368−372.

44. Gupte, A., and Buolamwini, J. K. (2004) Novel halogenated nitrobenzylthioinosine analogs as es nucleoside transporter inhibitors, *Bioorg. Med. Chem. Lett. 14*, 2257−2260.
45. Harley, E. R., Paterson, A. R., and Cass, C. E. (1982) Initial rate kinetics of the transport of adenosine and 4-amino-7-(beta-D-ribofuranosyl)pyrrolo[2,3-d]pyrimidine (tubercidin) in cultured cells, *Cancer Res. 42*, 1289−1295.
46. Paterson, A. R., Harley, E. R., and Cass, C. E. (1984) Inward fluxes of adenosine in erythrocytes and cultured cells measured by a quenched-flow method, *Biochem. J. 224*, 1001−1008.
47. Barile, M., Valenti, D., Passarella, S., and Quagliariello, E. (1997) 3′-Azido-3′-deoxythmidine uptake into isolated rat liver mitochondria and impairment of ADP/ATP translocator, *Biochem. Pharmacol. 53*, 913−920.
48. Barile, M., Brizio, C., De Virgilio, C., Delfine, S., Quagliariello, E., and Passarella, S. (1997) Flavin adenine dinucleotide and flavin mononucleotide metabolism in rat liver—the occurrence of FAD pyrophosphatase and FMN phosphohydrolase in isolated mitochondria, *Eur. J. Biochem. 249*, 777−785.
49. Lai, Y., Bakken, A. H., and Unadkat, J. D. (2002) Simultaneous expression of hCNT1-CFP and hENT1-YFP in Madin-Darby canine kidney cells. Localization and vectorial transport studies, *J. Biol. Chem. 277*, 37711−37717.
50. Mangravite, L. M., Lipshutz, J. H., Mostov, K. E., and Giacomini, K. M. (2001) Localization of GFP-tagged concentrative nucleoside transporters in a renal polarized epithelial cell line, *Am. J. Physiol. Renal Physiol. 280*, F879−885.
51. Mangravite, L. M., Xiao, G., and Giacomini, K. M. (2003) Localization of human equilibrative nucleoside transporters, hENT1 and hENT2, in renal epithelial cells, *Am. J. Physiol. Renal Physiol. 284*, F902−910.

BI0520535